ACADEMIC PRESS

Available online at www.sciencedirect.com
SCIENCE DIRECT®

NeuroImage

NeuroImage 19 (2003) 391–401

www.elsevier.com/locate/ynimg

# Automatic segmentation of thalamic nuclei from diffusion tensor magnetic resonance imaging

Mette R. Wiegell,[a,b,*] David S. Tuch,[a,c] Henrik B.W. Larsson,[b] and Van J. Wedeen[a]

[a] *Athinoula A. Martinos Center for Biomedical Imaging, Massachusetts General Hospital, 149 13th Street, Room 2301, Charlestown, MA 02129, USA*
[b] *Danish Research Center for Magnetic Resonance, Hvidovre Hospital, afd. 340, Kettegårds alle 30, 2650 Hvidovre, Denmark*
[c] *Harvard–MIT Division of Health Sciences and Technology, 77 Massachusetts Avenue, Cambridge, MA 02139, USA*

Received 21 February 2002; revised 2 December 2002; accepted 10 December 2002

**Abstract**

The nuclei of the thalamus have traditionally been delineated by their distinct cyto/myeloarchitectural appearance on histology. Here, we show that diffusion tensor magnetic resonance imaging (DTI) can noninvasively resolve the major thalamic nuclei based on the characteristic fiber orientation of the corticothalamic/thalamocortical striations within each nucleus. Using an automatic clustering algorithm, we extracted the Talairach coordinates for the individual thalamic nuclei. The center-of-mass coordinates for the segmented nuclei were found to agree strongly with those obtained from a histological atlas. The ability to resolve thalamic nuclei with DTI will allow for morphometric analysis of specific nuclei and improved anatomical localization of functional activation in the thalamus.


## Introduction

As the central relay station for the brain, the thalamus mediates communication among sensory, motor, and associative brain regions. The multiple functional pathways which relay through the thalamus form the thalamic cytoarchitecture. The thalamic cytoarchitecture is divided into functionally specific clusters referred to as nuclei.

The thalamic nuclei have traditionally been delineated by their distinct cyto- and myeloarchitectural appearance on histology (Smeets et al., 1999; Morel et al., 1997; Scannell et al., 1999; Van Buren and Borke, 1972). The number of thalamic nuclei reported with histological methods varies with the method employed, although most cyto/myeloarchitecture stains identify 14 major nuclei, with several subdivisions of the individual nuclei, some established by additional chemoarchitectural stains.

Thalamic changes have been implicated in a large number of diseases, including schizophrenia (Portas et al., 1998; Staal et al., 1998; Buchsbaum et al., 1999), Parkinson's disease (Giroux et al., 1998; de la Monte et al., 1989; McNeill et al., 1988; Samra et al., 1971; Xuereb et al., 1991), chronic pain syndrome (Davis et al., 1998), multiple sclerosis (Combarros et al., 1994), and wallerian degeneration (Ogawa et al., 1997). Parkinson's disease, multiple sclerosis, and chronic pain syndrome can also be treated by surgical ablation or electric stimulation (Tornqvist, 2001) of the involved nucleus. Presurgical planning of these cases often uses generic thalamic atlases to target the pertinent nucleus (Hardy et al., 1992; Nowinski, 1998; Otsuki et al., 1994; Tasker et al., 1991). Given the large degree of intersubject variability (Van Buren and Borke, 1972) in the location and size of the thalamic nuclei, such generic atlases may be highly inaccurate. Functional studies (fMRI, PET, SPECT) have also documented disease-related changes in functional activation of the thalamus (Blinkenberg et al., 2000; Heckers et al., 2000; Rauch et al., 2001; Rubia et al., 2001; Volz et al., 1999; Vuilleumier et al., 2001). However, due to the lack of a precise anatomical reference, these studies are generally not able to localize the activation to a specific nucleus within the thalamus.

The ability to resolve thalamic nuclei by noninvasive imaging would enable quantitative morphometric analysis of thalamic changes in the above-mentioned diseases, provide more accurate neurosurgical planning, and offer im-

* Corresponding author. Fax: +1-617-726-7422.
*E-mail address:* mette@nmr.mgh.harvard.edu (M.R. Wiegell).

1053-8119/03/$ – see front matter © 2003 Elsevier Science (USA). All rights reserved.
doi:10.1016/S1053-8119(03)00044-2

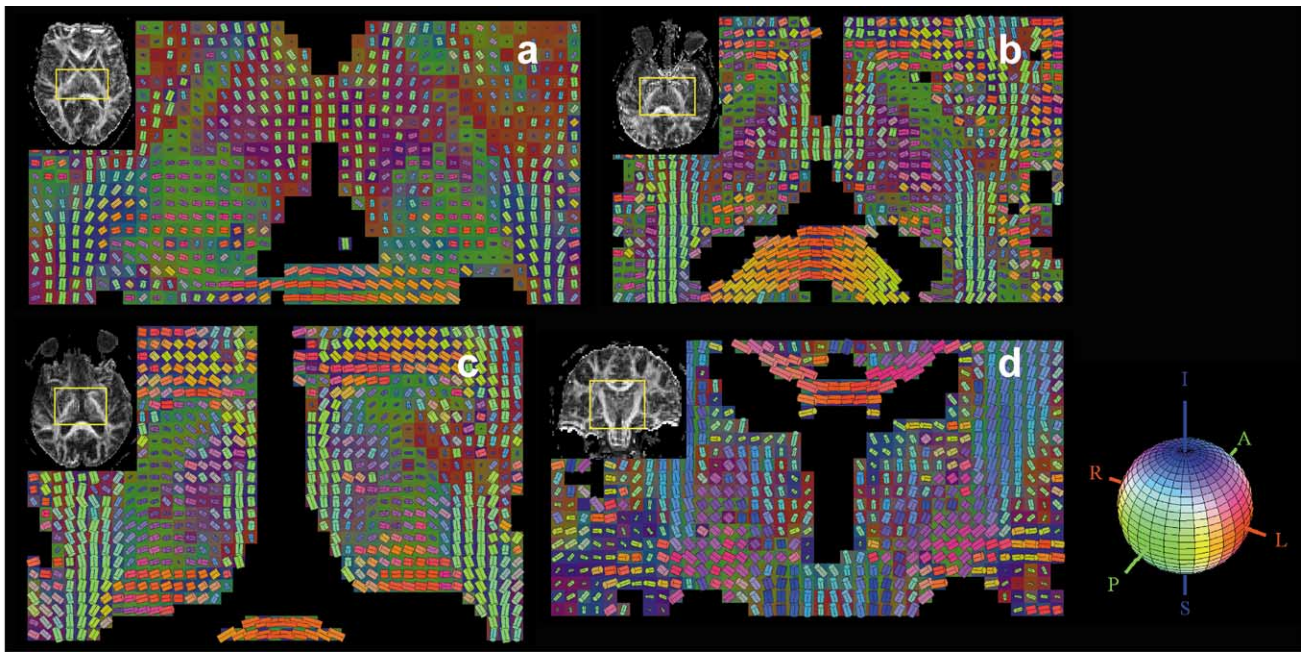


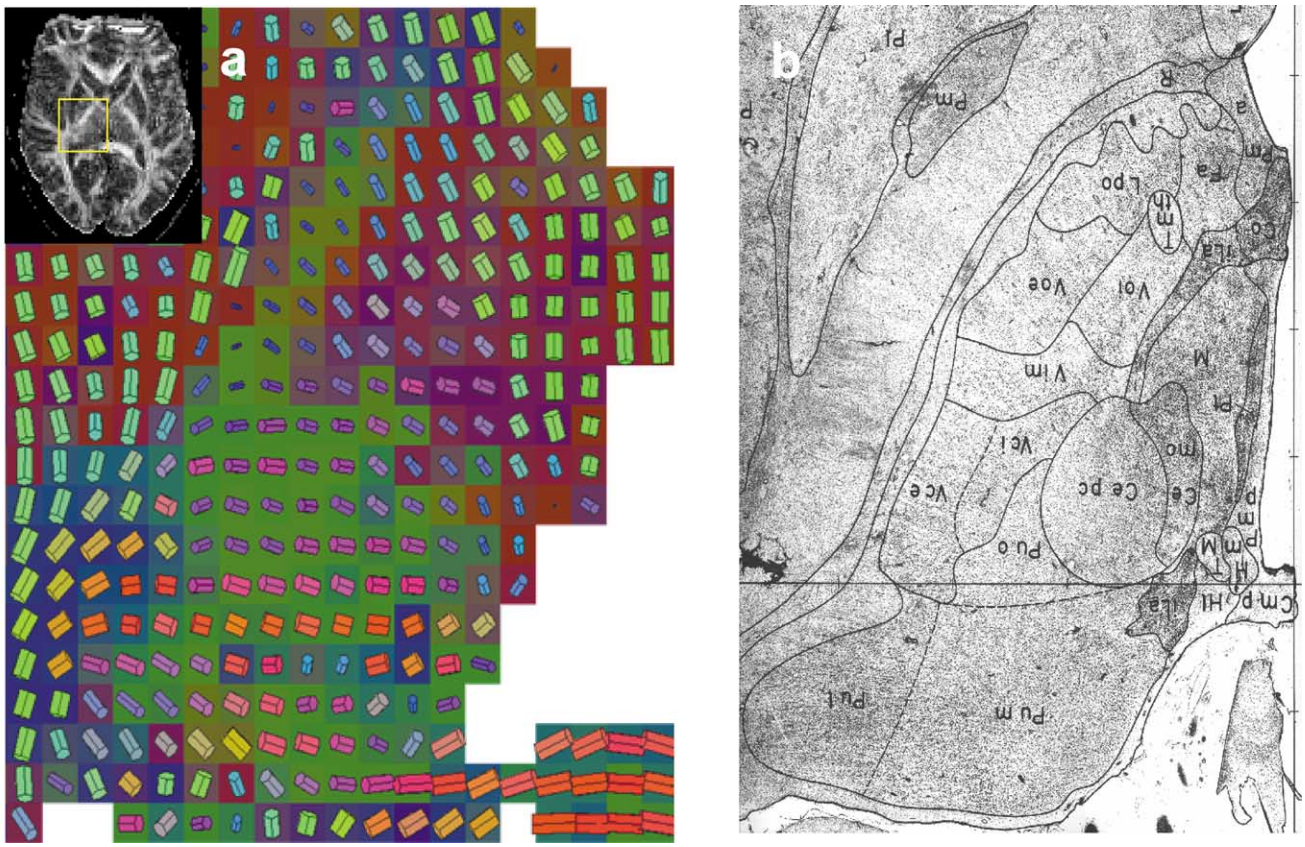


Fig. 1. Mid-thalamic diffusion tensor images of four subjects (a, b, c, d). Images a–c are axial slices and image d is a coronal slice at approximately mid-thalamic level. The region-of-interest (yellow box) for each subject is shown in the fractional anisotropy image (Pierpaoli and Basser, 1996) in the top left corner of the diffusion tensor image. In the diffusion tensor images, the cylinders depict the diffusion tensor within each voxel. The axes of each cylinder are oriented in the direction of the principal eigenvector of the local diffusion tensor. The length of the axes is scaled by the product of the corresponding eigenvalue and the square-root of the fractional anisotropy metric (Pierpaoli and Basser, 1996). The cylinders are colored by the direction of the principal eigenvector according to the red–green–blue sphere shown at bottom right with red indicating mediolateral, green anteroposterior, and blue superoinferior direction. The background slice is colored by the direction of the third eigenvector, an indicator of the sheet-normal direction (Wiegell et al., 2000a). Note how the clusters if mean fiber direction do not completely coincide with the clusters of mean sheet-normal direction.

Fig. 2. Histological comparison. (a) Diffusion tensor image (Fig. 1a) compared with a histological slice (b) from Van Buren and Borke (Van Buren and Borke, 1972) at a similar anatomical level. The region-of-interest (yellow box) is shown in the fractional anisotropy image (Pierpaoli and Basser, 1996) in the top left corner of the diffusion tensor image. Note the correspondence between diffusion orientation clusters and histologically defined nuclei borders.

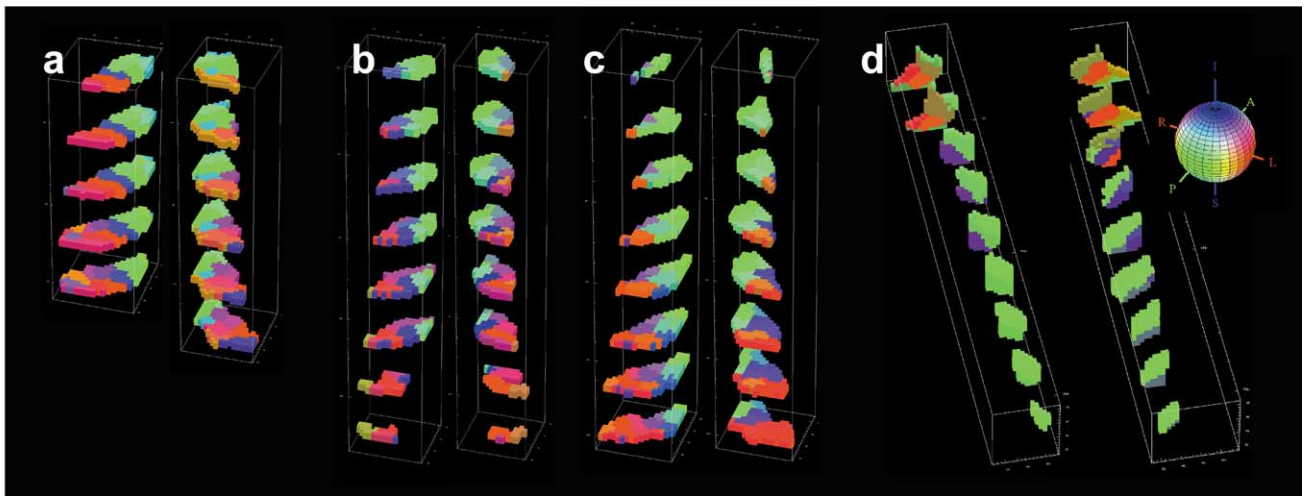


3

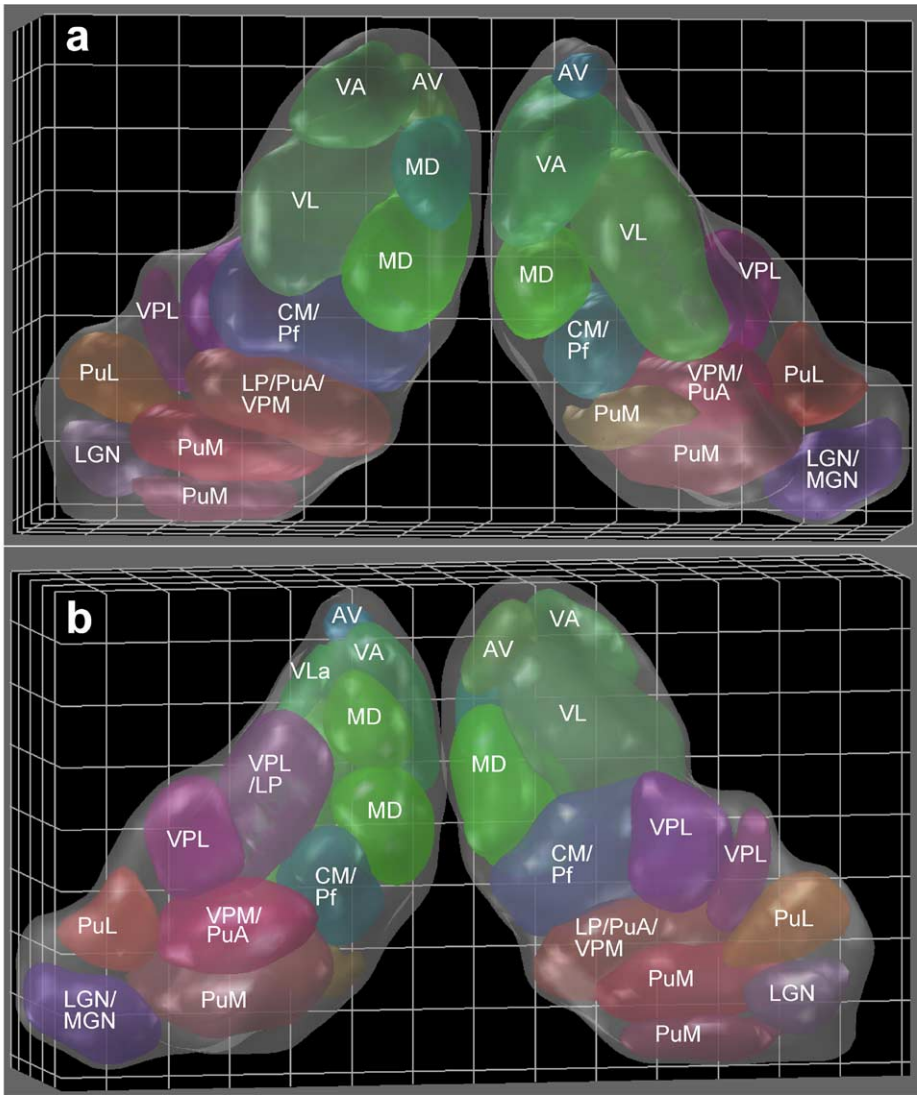


4

Fig. 3. Automatic segmentation results. Automatic segmentation results (a–d) for the left and right thalamic hemispheres of the four subjects, respectively. The clusters are color coded by the principal eigenvector of the mean diffusion tensor within each cluster (colorsphere in the upper right corner). The slices are artificially expanded by 11 mm for the axial data sets (a–c) and 19 mm for the coronal data set (d) in order to facilitate visualization. The coronal data set (d) is rendered front–anterior and back–posterior.

Fig. 4. Surface renderings of the automatic segmentation result from Fig. 3a. The clusters are color coded by the principal eigenvector of the mean diffusion tensor within each cluster. The two renderings show a superior view (a) and an inferior view (b), respectively.

proved anatomical localization of functional activation. Radiological identification of individual thalamic nuclei is not currently possible, however, as current imaging methods such as CT and conventional MR do not provide the necessary image contrast to differentiate the nuclei. Magnotta et al. (Magnotta et al., 2000) have shown that gray matter-nulled, inversion recovery T1-weighted MRI can identify the medialdorsal (MD) nucleus and the lateral portion based on the differences in white matter content, but further substructure was difficult to resolve. Furthermore, the T1 contrast between the nuclei was relatively small, with MD lower and the lateral portion higher in T1 signal (Holmes et al., 1998).

Previously, it has been proposed that the thalamic nuclei can be distinguished by their characteristic fiber orientation (Wiegell et al., 1999, 2000b; Niemann et al., 2000), a hereto unexploited distinction between the thalamic nuclei. This approach was motivated by the hypothesis that fiber orientations are relatively aligned within a nucleus due to fact that the cerebrocortical striations within a given nucleus all target the same region of cortex. Conventional MRI provides no information on the fiber orientation. However, diffusion tensor magnetic resonance imaging (DTI) can resolve the dominant fiber orientation within each image element (Basser and Pierpaoli, 1996; Hüppi et al., 1998; Jones et al., 1999; Lim et al., 1999; Neil et al., 1998; Pierpaoli et al., 1996; Shimony et al., 1999; Virta et al., 1999) by measuring the self-diffusion (i.e., Brownian motion) properties of the water molecules within the tissue. In tissues with strongly aligned microstructure such as brain or muscle (Basser et al., 1994; Cleveland et al., 1976; Garrido et al., 1994; Pierpaoli et al., 1996; Reese et al., 1995), diffusion is observed to be anisotropic (i.e., orientationally dependent) which is due to the diffusion barriers presented by cell membranes and/or macromolecules.

The direction of greatest diffusion measured by DTI parallels the dominant orientation of the tissue microstructure within each voxel. For example, the direction of greatest diffusion in cerebral white matter correlates strongly with the mean longitudinal direction of the axons (Pierpaoli et al., 1996; Hüppi et al., 1998; Makris et al., 1997; Neil et al., 1998; Peled et al., 1998). Diffusion anisotropy of white matter has furthermore been observed to depend on fiber heterogeneity (Virta et al., 1999; Wiegell et al., 2000a) and to increase with myelination (Neil et al., 1998; Rutherford et al., 1991; Sakuma et al., 1991; Takeda et al., 1997; Vorísek and Syková, 1997; Wimberger et al., 1995). In contrast, the diffusion tensor in cortical gray matter (Rise et al., 1993) has been shown to be isotropic and the same was thought to be true for subcortical gray matter structures. However, unlike other subcortical gray matter structures the thalamus contains both unmyelinated nerves and myelinated nerves. The unmyelinated nerves consist of intrathalamic relay and connections between the basal ganglia and the brain stem nuclei. The myelinated nerves are the thalamocortical striations, which provide sufficient diffusion restriction to be visible by DTI. Hence, we sought to test whether fiber orientation maps measured by DTI could distinguish the thalamic nuclei.

Using DTI we observed significant clusters of common fiber orientation in regions corresponding to the anatomical locations of the nuclei. Visual comparison with histological atlases (Duvernoy, 1991; Van Buren and Borke, 1972) showed correspondence between the location of the orientation clusters and the classically defined nuclei locations. In order to more accurately assess the diffusion tensor results we segmented the diffusion tensor data using a modified *k*-means clustering algorithm (Hartigan and Wong, 1979; Bishop, 1997).

The *k*-means algorithm is a classical statistical procedure for unsupervised clustering of data. The algorithm requires the user to specify a distance metric on the data space, the number of clusters thought to reside in the data, and the initial position of the cluster centroids. The centroids are points which are representative of the local neighborhood of the data. For each data point, the closest centroid is calculated and the data point is then associated with that centroid. Each centroid is then updated to the mean of the data points associated with that centroid. This procedure is repeated until the centroids do not change appreciably. Each cluster is then defined as the set of points closest to a centroid.

The distance metric in the present study used a weighted sum of the voxel distance and the diffusion tensor distance. The modified *k*-means clustering algorithm consequently finds voxels which are close in both position and diffusion. By defining the diffusion tensor distance term using the entire diffusion tensor and not solely, for example, the principal eigenvector, the clustering algorithm is sensitive to the entire structure of the diffusion tensor including both the primary and the secondary eigenstructures (Wiegell et al., 2000a).

The diffusion tensor data were segmented using the modified *k*-means algorithm. The center-of-mass (COM) coordinates for the segmented nuclei were then compared with previously reported center-of-mass coordinates from a Talairached histological atlas (Niemann et al., 2000). The diffusion tensor segmentation showed strong agreement with the histological data, providing support for the accuracy and robustness of the diffusion tensor method and the segmentation procedure.

## Materials and methods

### *Data acquisition*

Diffusion tensor MRI was obtained in healthy normal volunteers on a 1.5-T Siemens Vision Scanner at the Danish Research Center for Magnetic Resonance, Hvidovre Hospital, Denmark. The volunteers consented in accordance with the procedures of the Danish Ethical Committee. For each subject, data were acquired for 12 contiguous slices cover-

ing the whole thalamus and oriented either axially or coronally. We used a single-shot SE-DWI-EPI sequence, with TE 101 ms, TR 4 s, matrix size 128 × 128, FOV 230 mm, slice thickness 3 mm, 36 averages. The diffusion-encoding parameters were $\delta = 28.9$ ms, $\Delta = 51.9$ ms, and diffusion time 42.6 ms, gradient strength 12 mT/m, which gave an approximate *b*-factor of 550 s/mm$^2$, calculated analytically taking preparation and imaging gradients into account (Mattiello et al., 1997). One null image and six diffusion weighted images were obtained with the diffusion-encoding gradients directed along the following axes ($\pm$1,1,0), ($\pm$1,0,1), and (0,$\pm$1,1). The SNR obtained in the nonaveraged unattenuated diffusion weighted image was approximately 15, resulting in a SNR for the averaged DW images of approximately 90. The images were realigned to compensate for eddy-current-induced morphing in the phase and readout directions, although eddy-currents were only detected in the phase direction. Images with motion artifacts were excluded. The eigensystem of the diffusion tensor was calculated on a voxel-by-voxel basis (Mattiello et al., 1997).

*Manual delineation of the thalamus*

The thalamic volumes were hand-segmented using the color-coded DTI maps of the first eigenvector and the T2 weighted images. The thalamus was defined medially by the third ventricle and laterally by the posterior limb of the internal capsule, superiorly by the lateral ventricles and inferiorly by the brainstem. The lateral boundary was defined by the posterior limb of the internal capsule which, using the color-coded DTI maps of the first eigenvector, is well-defined as a blue diagonal band lateral to the thalamus. The inferior/ventral boundary was defined anteriorly by the anterior commissure, the optic chiasm, and the caudal edge of the mammillary bodies and posteriorly by the cerebral peduncles and thus included parts of the geniculate nuclei.

*Automatic segmentation procedure*

The thalamic nuclei were clustered separately for each hemisphere using the *k*-means clustering algorithm (Hartigan and Wong, 1979; Bishop, 1997). In general, the *k*-means algorithm requires four specifications: (1) the number of clusters, (2) a distance metric, (3) initialization of the cluster centroids, and (4) a convergence criterion.

*Number of clusters*

The number of nuclei (clusters) was set a priori to $n = 14$ per hemisphere based on preliminary visual inspection of the diffusion tensor icon renderings (as in Fig. 1).

*Distance metric*

The distance between voxels was defined as a linear combination of the Mahalanobis voxel distance and the Frobenius tensor distance. More specifically, the position-diffusion-tensor distance $E_{jk}$ between a voxel $j$ and a centroid $k$ was taken as a linear combination of the voxel position distance and the diffusion tensor distance, i.e.,

$$E_{jk} = \|\mathbf{x}_j - \bar{\mathbf{x}}_k\|_{\mathbf{W}_k} + \gamma\|\mathbf{D}_j - \bar{\mathbf{D}}_k\|,$$

where $\mathbf{x}_j$ is the location of voxel $j$, $\bar{\mathbf{x}}_k$ is the mean voxel location for cluster $k$, $\mathbf{W}_k$ is the covariance matrix for the voxels in cluster $k$, $\gamma$ is a weighting factor to control the tradeoff between the diffusion tensor distance and the voxel distance, $\mathbf{D}_j$ is the diffusion tensor for voxel $j$, and $\bar{\mathbf{D}}_k$ is the mean diffusion tensor for cluster $k$. The norm on the voxel location is the Mahalanobis norm defined as $\|\mathbf{x}\|_{\mathbf{W}} = (\mathbf{x}^T\mathbf{W}^{-1}\mathbf{x})^{1/2}$ and the norm on the diffusion tensor is the Frobenius norm defined as $\|\mathbf{F}\| = [\mathrm{Tr}(\mathbf{F}^T\mathbf{F})]^{1/2}$, where Tr is the trace of tensor $\mathbf{F}$. The Mahalanobis norm was used instead of the Euclidean norm to prevent geometric bias toward spherical clusters. The covariance matrices $\mathbf{W}_k$ were recalculated at every iteration. The weighting factor $\gamma$ was calculated for each subject using the formula

$$\gamma = \{\mathrm{Tr}[\boldsymbol{\Sigma}(\mathbf{x})]\}/\{\mathrm{Tr}[\boldsymbol{\Sigma}(\mathbf{d})]\}^{1/2}$$

where $\Sigma(\mathbf{x})$ is the covariance matrix for the voxel locations, and $\Sigma(\mathbf{d})$ is the covariance matrix for the flattened diffusion tensors $\mathbf{d} = [D_{11}\ D_{12}\ D_{13}\ D_{12}\ D_{22}\ D_{23}\ D_{13}\ D_{23}\ D_{33}]^T$. The weighting factor $\gamma$ controls the tradeoff between the voxel location distance and the diffusion tensor distance. The tradeoff is accomplished by normalizing the respective distance terms by the observed deviation of each variable.

*Initialization of the cluster centroids*

The $n$ centroid locations were initialized along each side of a line segment passing from the posterior tip of the thalamic hemisphere through the center-of-mass to the anterior tip within the plane spanned by the first and second eigenvectors of the voxel location covariance matrix. The clustering results were strongly reproducible using other centroid initialization schemes provided that the initialization was sufficiently spatially uniform.

*Convergence criterion*

The clustering routine was iterated until no centroid moved more than 0.1 mm, i.e., until $\max_k\|\Delta\bar{\mathbf{x}}_k\| < 0.1$ mm.

*Nuclei identification*

Following Niemann (Niemann et al., 2000), 12 nuclei (17 in total including subdivisions) were assigned to the clusters. The nuclei, including the subdivisions in square brackets, were AV, MD, LD, LP, VA, VL [VLa, VLp], VPM, VPL, CM, Pu [PuA, PuM, PuL], LGN, and MGN, respectively. The nuclei were assigned to 14 clusters per hemisphere based on the location, shape, size, and mean diffusion orientation of the segmentation cluster. The nuclei were anatomically labeled by one of the investigators (MRW) who was blind to the COM information from the Niemann et al. study (Niemann et al., 2000). The anatomical

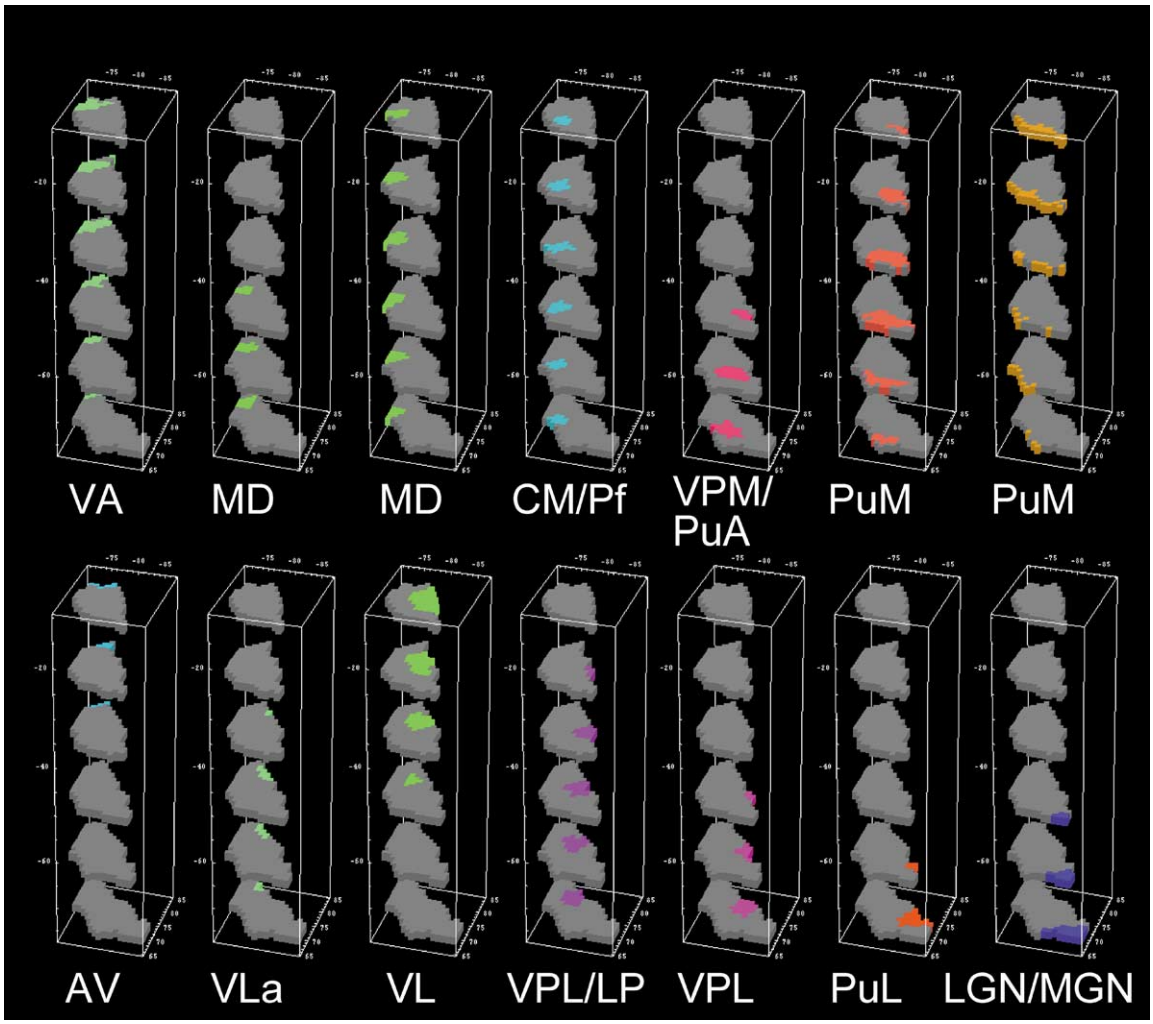


Fig. 5. Segmented nuclei. Fourteen segmented nuclei for left thalamic hemisphere of subject a. The segmented nucleus is colored by the principal eigenvector and the remainder of the thalamus is colored gray. As for Fig. 3, the slices are artificially expanded to facilitate visualization.

Table 1
Mean fiber orientation of each of the individually segmented nuclei from each subject

| | Subject 1 | | Subject 2 | | Subject 3 | | Subject 4 | |
|---|---|---|---|---|---|---|---|---|
| Hemisphere | Right | Left | Right | Left | Right | Left | Right | Left |
| AV | | | | | | | | |
| MD | | | | | | | | |
| LD | | | | | | | | |
| LP | | | | | | | | |
| VA | | | | | | | | |
| VL | | | | | | | | |
| VLa | | | | | | | | |
| VLp | | | | | | | | |
| VPL | | | | | | | | |
| VPM | | | | | | | | |
| MGN | | | | | | | | |
| LGN | | | | | | | | |
| CM | | | | | | | | |
| Pu | | | | | | | | |
| PuM | | | | | | | | |
| PuA | | | | | | | | |
| PuL | | | | | | | | |

*Note.* Color representation: red, mediolateral; green, anteroposterior; and blue, superoinferior. Cells containing two half-cells indicate nuclei for which two segmentation clusters were assigned.

labeling was based on the depictions of nucleus location, shape, size, and fiber orientation provided by the atlases of Duvernoy (Duvernoy, 1991), Van Buren (Van Buren and Borke, 1972), and Morel (Morel et al., 1997). If a cluster was assigned to a nucleus, which contained subdivisions, but the assignment to a particular subdivision could not be made, then the cluster was assigned to the undifferentiated nucleus. For example, if a cluster belonged to VL but could not be assigned definitely to VLa or VLp it was assigned to VL. If a cluster subsumed 2 anatomical nuclei then the cluster was assigned to both nuclei, and the center-of-mass and volume statistics were attributed to both nuclei. If multiple clusters were consistent with the same nucleus, then all of the clusters were assigned to that nucleus. In that case, the COM and volume statistics were taken from the cluster which agreed most strongly in morphometry and location with the nucleus used by Niemann (AV, CM, LP, MDmc MGN, PuA, VLa, and VPLa, respectively).

*Center-of-mass comparison*

Eight nuclei (AV, CM, LP, MDmc, MGN, PuA, VLa, and VPLa) of the 13 reported nuclei COM coordinates from Niemann (Niemann et al., 2000) were used for the center-of-mass comparison. Of the 5 remaining nuclei, the red nucleus and the subthalamic nucleus were outside the area considered in this paper; the habenular nucleus and the ventromedial nucleus were deemed too small for detection with our present spatial image resolution, and the parafascicular nucleus was considered part of the centromedian–parafascicular nuclei complex. The center-of-mass coordinates for the segmented nuclei were registered to Talairach space (Talairach et al., 1957) using the AC–PC plane as a landmark and then scaled in the Talairach frame to account for AC–PC distance variability as was done by Niemann et al. (Niemann et al., 2000). The corrected Talairach coordinates were then pooled over the subjects ($N = 4$). The corrected COM coordinates reported by Niemann were obtained by digitally scanning the published data (Niemann et al., 2000) and likewise pooling over the subjects ($N = 2$). The agreement between the segmentation and the Niemann COM coordinates was assessed with a multivariate ANOVA test at a significance level of 0.05.

## Results

The mean volume of the thalamus determined from the structural images was 7108 ± 918 $mm^3$ (per hemisphere), and the mean distance from the anterior commisure to the posterior commisure (AC–PC) was 28.4 ± 3.3 mm. The volume of the left thalamic hemisphere was 7141 ± 530 $mm^3$ and that of the right hemisphere was 7073 ± 457 $mm^3$. The diffusion tensor data were visualized as cylindrical icon fields against a background color-coded according to the direction of the sheet-normal vector (the third eigenvector) (Wiegell et al., 2000a) (Fig. 1). The mean fractional anisotropy (FA) (Pierpaoli and Basser, 1996) over the thalamic volume was 0.364 ± 0.007.

The diffusion tensor images showed clusters of common fiber orientation corresponding to the direction of the corticothalamic and thalamocortical striations within each nucleus. The sheet-normal direction also exhibited clustering that did not always coincide with the clustering suggested by the mean fiber direction. The location of the fiber orientation clusters defined by both the fiber and the sheet directions corresponded generally with the location of the nuclei provided by histological atlases (Fig. 2).

Each of the 14 segmentation clusters (Figs. 3 and 4) was assigned to anatomical nuclei according to the criteria described under Materials and Methods (Fig. 5). The location, size, and shape of the segmented nuclei were consistent with Morel's stereotactic atlas (Morel et al., 1997). The relative location of the clusters within an individual thalamus was consistent between subjects, but the cluster locations and morphometry varied between subjects. The mean orientation of fibers within each nucleus showed high correlation between subjects (Table 1). The agreement between the segmentation and the Niemann (Niemann et al., 2000) center-of-mass coordinates was assessed with a multivariate anova test (Fig. 6). For six (AV, CM, LP, MGN, PuA, and VPLa) of the 8 nuclei (AV, CM, LP, MD, VLa, MGN, PuA, and VPLa) specified by Niemann we were not able to reject the null hypothesis (at a 0.05 significance level) that the COM coordinates were the same for the DTI and histological segmentations. For these six nuclei, the $P$ values were AV ($P = 0.526$), CM ($P = 0.623$), LP ($P = 0.481$), MGN ($P = 0.357$), PuA ($P = 0.436$), and VPLa ($P = 0.433$). Hence, for these nuclei the COM coordinates obtained from DTI and from the Niemann atlas were not significantly different. The COM coordinates for the MD and VLa nuclei did not significantly agree ($P < 0.05$) with the COM coordinates provided by the Niemann atlas.

From Table 1 it can be appreciated that the diffusion orientations of the individual nuclei correspond to their respective corticothalamic and thalamocortical striations (Table 2). For example, the MD nuclei has an anteroposterior direction corresponding to the direction of its projections to the frontal association cortices through the anterior limb of the internal capsule. Likewise, the ventrolateral (VL) nucleus exhibits anteroposterior direction although with a superoinferior tendency (more blue color), corresponding to the direction of the striations to the premotor and primary motor cortices through the anterior limb of the internal capsule.

The ventroposterior nucleus, often subdivided into two nuclei, the ventral posterolateral (VPL) and ventral posteromedial (VPM), exhibited almost the same orientation. Both nuclei receive input from the spinal cord, the brainstem, and the medial lemniscus and project to primary somatic sensory cortex. The two nuclei differ, however, in their target areas, body and head, respectively, in addition to projec-

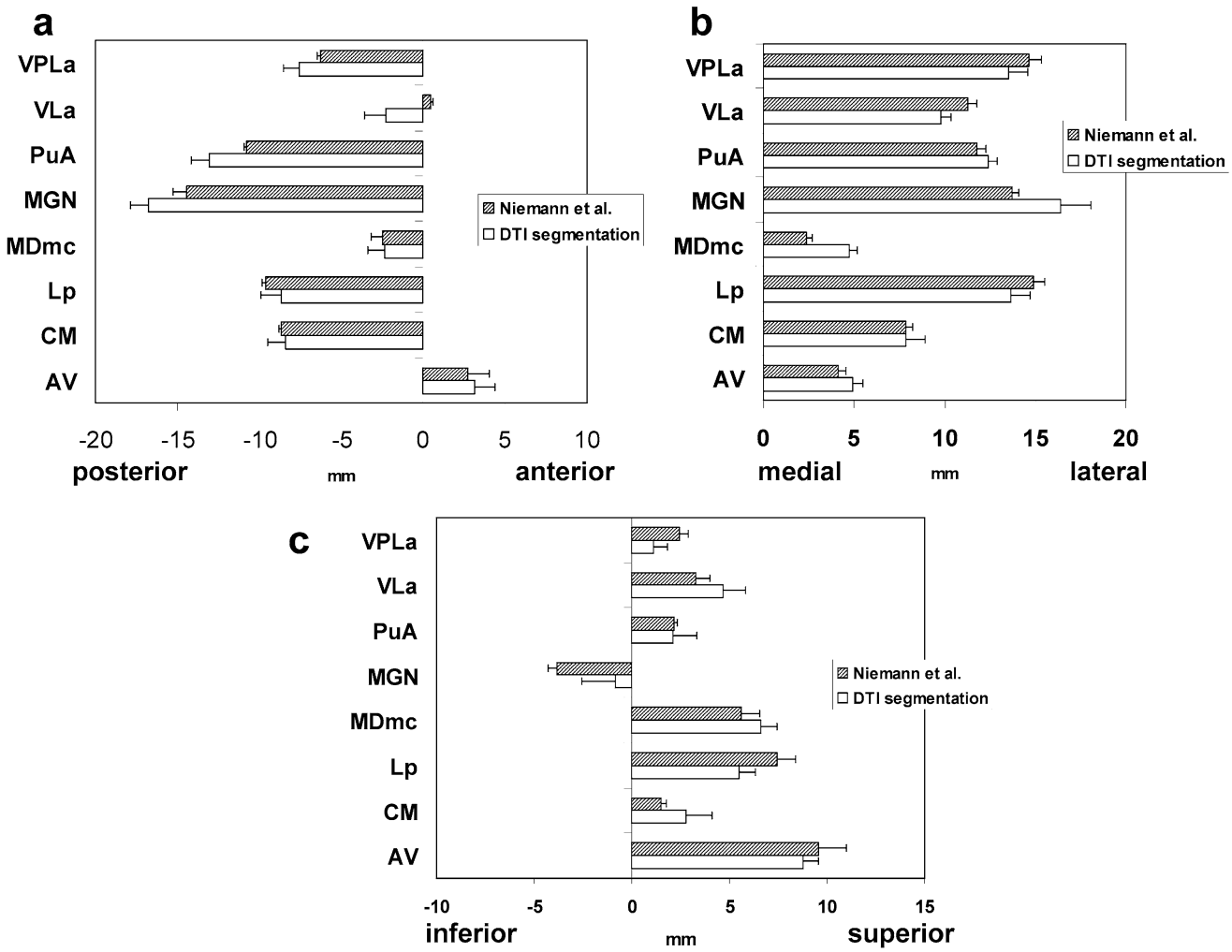


Fig. 6. Comparison between center-of-mass (COM) coordinates obtained from Niemann and DTI segmentation. (a) Anteroposterior direction, (b) mediolateral direction, and (c) superoinferior direction, respectively.

tions to the insula cortex from VPM. This is reflected in the orientations of the two nuclei with both nuclei showing superoinferior and mediolateral orientation corresponding to the striations through the posterior limb of the internal capsule. Where VPM was identified, the nucleus showed orientations more mediolateral than those of VPL, confirming the additional projection to the insula cortex.

Of the intralaminar nuclei, the centro median (CM) and the parafascilus nuclei (PF) complex were identified. The nuclei which belong to the class of diffuse projecting nuclei regulate the cortical activity by accommodating input from the brainstem, basal ganglia, and spinal cord to, respectively, the motor cortex and putamen (CM) and the prefrontal cortex and the caudate nucleus (PF). Both nuclei displayed orientations in the superoinferior and slightly anterior direction.

The largest thalamic nuclei, the pulvinar nucleus, facilitates bidirectional connections to the parietal, temporal, and occipital association cortex. These projections occur lateral to the optic radiation and spread out to the cortical areas via the posterior thalamic peduncle. In accordance with these projections, the observed primary orientation of the pulvinar was mediolateral, which distinguished it from all other thalamic nuclei.

## Discussion

Using DTI we were able to identify and automatically segment the major nuclei of the thalamus. The diffusion tensor segmentation results agreed strongly with a previously published histological study conducted by Niemann et al. (Niemann et al., 2000) for the AV, CM/PF, and LP nuclei. Specifically, the COM coordinates of the AV, CM, LP, MGN, PuA, and VPLa nuclei provided by the automatic DTI segmentation agreed strongly with the COM coordinates provided by the Niemann atlas. Further, the fiber directions within these nuclei, as determined by the principal eigenvector of the diffusion tensor, were consistent with

Table 2
Known thalamic output pathways: thalamic nuclei with their specific output projections and cortical target areas

| Principal nucleus/nuclei | Functional class | Major cerebral outputs | Cerebral pathway | Functions |
|---|---|---|---|---|
| Anterior (A) | Relay | Cingulate gyrus, limbic association cortex | Anterior limb of internal capsule, anterior thalamic peduncle | Learning, memory, and emotions |
| Media dorsal (MD) | Association | Prefrontal association cortex | Anterior limb of internal capsule, anterior thalamic peduncle | Emotions, cognition, learning and memory, affect, and foresight |
| Lateral dorsal (LD) | Relay | Cingulate gyrus | Anterior limb of internal capsule, anterior thalamic peduncle | |
| Lateral posterior (LP) | Association | Posterior parietal association cortex | Superior thalamic peduncle | Sensory integration |
| Pulvinar (Pu) | Association | Parietal, temporal, occipital association cortex | Along optic radiation, posterior thalamic peduncle | Sensor integration, perception, language, visual orientation, and attention |
| Ventral anterior (VA) | Relay | Supplementary motor cortex | Genu and posterior limb of internal capsule, superior thalamic peduncle | Movement planning |
| Ventrolateral (VL) | Relay | Premotor and primary motor cortex | Genu and posterior limb of internal capsule, superior thalamic peduncle | Movement planning and control |
| Ventral posterolateral (VPL) | Relay | Primary somatosensory cortex | Posterior limb of internal capsule, superior thalamic peduncle | In the body: touch, limb position sense, pain, and temperature sense |
| Ventral posteromedial (VPM) | Relay | Primary somatosensory cortex, insula | Posterior limb of internal capsule, superior thalamic peduncle | In the head: touch, limb position sense, pain, and temperature sense |
| Medial geniculate (MGN) | Relay | Primary auditory cortex, superior temporal gyrus | Sublenticular part of the internal capsule (temporopontine tract), auditory radiation | Hearing |
| Lateral geniculate (LGN) | Relay | Primary visual cortex, calcarine sulcus | Retrolenticular part of the internal capsule (occipitopontine tract), optic radiation | Vision |
| Centromedian (CM) | Diffuse projecting | Motor cortex, putamen | | Regulation of cortical activity |
| Parafascicular (PF) | Diffuse projecting | Prefrontal cortex, caudate nucleus | | Regulation of cortical activity |
| Central lateral | Diffuse projecting | Cerebral cortex, basal ganglia | | Regulation of cortical activity |
| Midline nuclei | Diffuse projecting | Cerebral cortex, basal forebrain, allocortex | | Regulation of forebrain neuronal excitability |
| Reticular nucleus | | Thalamus | Inhibitory | Regulation of thalamic neuronal activity |

the known orientations of the corticothalamic and thalamocortical projections.

However, for MD and VLa, the COM coordinates obtained for the DTI and the histological atlas were significantly different. The relatively weaker agreement for these nuclei is most likely due to the fact that these nuclei are complexes which contain further subnuclei, as reported by Niemann. The COM comparison was performed between these nuclear complexes and the Niemann subnuclei which represents an anatomical discrepancy. For example, Niemann specified the COM for VLa which we compared to the COM for the full VL complex which consists of both VLa and VLp. This is further borne out by the fact that the COM locations for VL and VLa agreed more strongly in the superoinferior direction than in the anteroposterior and mediolateral directions.

The discrepancy may also be due to intersubject variability in the location of the nuclei (Van Buren and Borke, 1972). Moreover, intersubject variability in the overall volume and morphometry of the thalamus may introduce a bias in the scaling correction. Following Niemann the COM coordinates were scaled in all Talairach dimensions by the AC–PC distance in order to reduce the intersubject variability. However, scaling all dimensions by the AC–PC distance will not in general account for the full variability of the thalami. This is reflected, for example, in the stronger agreement in the AP dimension for the COM locations.

The difference between the segmented and histological COM coordinates may also be due to the material distortions introduced by extraction and fixation of the tissue for the histology. This point is supported by the generally larger volumes reported in living subjects by MRI ($7108 \pm 918$ $mm^3$ reported here and $8.65 \pm 0.95$ $mm^3$ reported by Collins et al., 1998) as opposed to fixed tissue specimens (6625 $mm^3$, Niemann and van Nieuwenhofen, 1999).

Despite the above differences, we were able to reliably segment a number of the major nuclei. For example, in all subjects we identified the AV, MD, LP, VA, VL [VLa, VLp], VPL, CM, Pu [PuA, PuM, PuL], LGN, and MGN nuclei from the 14 segmented classes and in three of four subjects the LD and VPM nuclei were also identified. The COM coordinates obtained from the automatic segmentation were in strong agreement with the COM results reported by Niemann, with the exception of the MDmc and

VLa nuclei. All segmented nuclei exhibited mean fiber orientations which were consistent between subjects and correlated with the orientation of their known corticothalamic and thalamocortical projections. In general the antero superior portion of the thalamus showed anteroposterior directed fiber populations, the lateral portion showed superoinferior and mediolateral directions, and the posterior portion of the thalamus showed mediolateral directions. The orientation of each segmented nucleus varied as a function of the specific cortical target of the nucleus.

For the present study the number of nuclei was specified a priori based on the number of clusters which could be visually identified in the data set. Further work will be necessary to incorporate an automatic procedure for determining the number of nuclei. Given the hierarchical organization of the thalamic nuclei it would also be of interest to examine the thalamic parcellation as a function of the number of specified nuclei.

To our knowledge, this is the first report of anatomically significant diffusion anisotropy in a human gray matter structure. The observed anisotropy in the thalamus is most likely due to the thalamocortical and corticothalamic projections which are myelinated, and not the shorter, mostly unmyelinated interthalamic, striatal, and brainstem projections. The attribution of the observed anisotropy to the thalamocortical/corticothalamic projections is prompted by the agreement between the observed fiber directions and the directions of these projections. These projections pass through the internal capsule and the corona radiata, from which they detach into the thalamic peduncles in an orderly fashion. Most of the projections connect to the thalamus at the rostral and caudal poles as well as along the dorsal surface. However, based on the present data we cannot rule out the possibility that unmyelinated structures contributed to the observed diffusion anisotropy.

The ability to identify the thalamic nuclei could be of importance for the diagnosis of diseases with thalamic involvement. Of special interest would be long-term effects and possible subsequent reorganizations of the thalamic nuclei in order to adapt to novel environments, as was recently shown to occur in monkeys (Jones and Pons, 1998). A combination of diffusion tensor imaging and functional MRI could help elucidate the functional relations within and between the thalamic nuclei.

## Acknowledgments

The authors thank Katja Krabbe, M.D., for help during the data acquisition, and Bruce Fischl, Ph.D., for helpful comments on the segmentation algorithm. M.R. Wiegell, Ph.D., was funded in part through Apotekerfonden af 1991, Denmark, and through NIH Grant No. 5RO1 NS 38477-02. The authors acknowledge the NIH for funding via NIH Grant 1RO1 MH 64044 A 01.

## References

Basser, P.J., Mattiello, J., LeBihan, D., 1994. MR diffusion tensor spectroscopy and imaging. Biophys. J. 66, 259–267.

Basser, P.J., Pierpaoli, C., 1996. Microstructural and physiological features of tissues elucidated by quantitative-diffusion-tensor MRI. J. Magn. Reson. B. 111, 209–211.

Bishop, C.M., 1997. Neural Networks for Pattern Recognition. Oxford Press, New York.

Blinkenberg, M., Rune, K., Jensen, C.V., Ravnborg, M., Kyllingsbaek, S., Holm, S., Paulson, O.B., Sorensen, P.S., 2000. Cortical cerebral metabolism correlates with MRI lesion load and cognitive dysfunction in MS. Neurology 54, 558–564.

Buchsbaum, M.S., Byne, W., Hazlett, E.A., Shihabuddin, L., Tang, C.Y., Wei, T.-C., Haznedar, M., Siever, L.J., 1999. PET, MRI, and postmortem studies of the thalamus in schizophrenia. Proceedings of the Fifth International Conference on Functional Mapping of the Human Brain 639.

Cleveland, G.G., Chang, D.C., Hazlewood, C.F., 1976. Nuclear magnetic resonance measurements of skeletal muscle. Anisotropy of the diffusion coefficient of the intracellular water. Biophys. J. 16, 1043–1053.

Collins, D.L., Kabani, N.J., Evans, A.C., 1998. Automatic volume estimation of gross cerebral structures. Proceedings of the Fourth International Conference of Functional Mapping of the Human Brain 702.

Combarros, O., Miró, J., Berciano, J., 1994. Ageusia associated with thalamic plaque in multiple sclerosis. Eur. Neurol. 34, 344–346.

Davis, K.D., Kwan, C.L., Crawley, A.P., Mikulis, D.J., 1998. Functional MRI study of thalamic and cortical activations evoked by cutatenous heat, cold, and tactile stimuli. J. Neurophys. 80, 1533–1546.

de la Monte, S.M., Wells, S.E., Hedley-Whyte, E.T., Growdon, J.H., 1989. Neuropathological distinction between Parkinson's dementia and Parkinson's plus Alzheimer's disease. Ann. Neurol. 26, 309–320.

Duvernoy, H., 1991. The Human Brain. Surface, Three-Dimensional Sectional Anatomy and MRI. Springer-Verlag, New York.

Garrido, L., Wedeen, V.J., Kwong, K.K., Spencer, U.M., Kantor, H.L., 1994. Anisotropy of water diffusion in the myocardium of the rat. Circ. Res. 74, 789–793.

Giroux, M.L., Grafton, S.T., Votaw, J.R., DeLong, M.L., Hoffman, J.M., 1998. Medication related changes in cerebral glucose metabolism in Parkinson's disease. Proceedings of the Fourth International Conference on Functional Mapping of the Human Brain 237.

Hardy, T.L., Smith, J.R., Brynildson, L.R., Flanigan, H.F., Gray, J.G., Spurlock, D., 1992. Magnetic resonance imaging and anatomic atlas mapping for thalamotomy. Stereotact. Funct. Neurosurg. 58, 30–32.

Hartigan, J.A., Wong., M.A., 1979. A k-means clustering algorithm. Appl. Statist. 28, 100–108.

Heckers, S., Curran, T., Goff, D., Rauch, S.L., Fischman, A.J., Alpert, N.M., Schacter, D.L., 2000. Abnormalities in the thalamus and prefrontal cortex during episodic object recognition in schizophrenia. Biol. Psychiatry 48, 651–657.

Holmes, C.J., Hoge, R., Collins, L., Woods, R., Toga, A.W., Evans, A.C., 1998. Enhancement of MR images using registration for signal averaging. J. Comput. Assist. Tomogr. 22, 324–333.

Hüppi, P.S., Maier, S.E., Peled, S., Zientara, G.P., Barnes, P.D., Jolesz, F.A., Volpe, J.J., 1998. Microstructural development of human newborn cerebral white matter assessed in vivo by diffusion tensor magnetic resonance imaging. Pediatr. Res. 44, 584–590.

Jones, D.K., Simmons, A., Williams, S.C. R., Horsfield, M.A., 1999. Non-invasive assessment of axonal fiber connectivity in the human brain via diffusion tensor MRI. Magn. Reson. Med. 42, 37–41.

Jones, E.G., Pons, T.P., 1998. Thalamic and brainstem contributions to large-scale plasticity of primate somatosensory cortex [see comments]. Science 282, 1121–1125.

Lim, K.O., Hedehus, M., Moseley, M., de Crespigny, A., Sullivan, E.V., Pfefferbaum, A., 1999. Compromised white matter tract integrity in schizophrenia inferred from diffusion tensor imaging. Arch. Gen. Psych. 56, 367–374.

Magnotta, V.A., Gold, S., Andreasen, N.C., Ehrhardt, J.C., Yuh, W.T., 2000. Visualization of subthalamic nuclei with cortex attenuated inversion recovery MR imaging [In Process Citation]. NeuroImage 11, 341–346.

Makris, N., Worth, A.J., Sorensen, A.G., Papadimitriou, G.M., Wu, O., Reese, T.G., Wedeen, V.J., Davis, T.L., Stakes, J.W., Caviness, V.S., Kaplan, E., Rosen, B.R., Pandya, D.N., Kennedy, D.N., 1997. Morphometry of in vivo human white matter association pathways with diffusion-weighted magnetic resonance imaging. Ann. Neurol. 42, 951–962.

Mattiello, J., Basser, P.J., Le Bihan, D., 1997. The b matrix in diffusion tensor echo-planar imaging. Magn. Reson. Med. 37, 292–300.

McNeill, T.H., Brown, S.A., Rafols, J.A., Shoulson, I., 1988. Atrophy of medium spiny 1 striatal dentrites in advanced Parkinson's disease. Brain Res. 455, 148–152.

Morel, A., Magnin, M., Jeanmonod, D., 1997. Multiarchitectonic and stereotactic atlas of the human thalamus. J. Comp. Neurol. 387, 588–630.

Neil, J.J., Shiran, S.I., McKinstry, R.C., Schefft, G.L., Snyder, A.Z., Almli, C.R., Akbudak, E., Aronovitz, J.A., Miller, J.P., Lee, B.C. P., Conturo, T.E., 1998. Normal brain in human newborns: apparent diffusion coefficient and diffusion anisotropy measured by using diffusion tensor MR imaging. Radiology 209, 57–66.

Niemann, K., Mennicken, V.R., Jeanmonod, D., Morel, A., 2000. The Morel stereotactic atlas of the human thalamus: atlas-to-MR registration of internally consistent canonical model. NeuroImage 12, 601–616.

Niemann, K., van Nieuwenhofen, I., 1999. One atlas — three anatomies: relationships of the Schaltenbrand and Wahren microscopic data. Acta Neurochir. (Wien) 141, 1025–1038.

Nowinski, W.L., 1998. Anatomical targeting in functional neurosurgery by the simultaneous use of multiple Schaltenbrand–Wahren brain atlas microseries. Stereotact. Funct. Neurosurg. 71, 103–116.

Ogawa, T., Yoshida, Y., Okudera, T., Noguchi, K., Kado, H., Uemura, K., 1997. Secondary thalamic degeneration after cerebral infarction in the middle cerebral artery distribution: evaluation with MRI imaging. Radiology 204, 255–262.

Otsuki, T., Jokura, H., Takahashi, K., Ishikawa, S., Yoshimoto, T., Kimura, M., Yoshida, R., Miyazawa, T., 1994. Stereotactic gamma-thalamotomy with a computerized brain atlas: technical case report. Neurosurgery 35, 764–767 discussion 767–768.

Peled, S., Gudbjartsson, H., Westin, C.-F., Kikinis, R., Jolesz, F.A., 1998. Magnetic resonance imaging shows orientation and asymmetry of white matter fiber tracts. Brain Res. 780, 27–33.

Pierpaoli, C., Basser, P.J., 1996. Toward a quantitative assessment of diffusion anisotropy. Magn. Reson. Med. 36, 893–906.

Pierpaoli, C., Jezzard, P., Basser, P.J., Barnett, A., Di Chiro, G., 1996. Diffusion tensor MR imaging of the human brain. Radiology 201, 637–648.

Portas, C.M., Goldstein, J.M., Shenton, M.E., Hokama, H.H., Wible, C.G., Fischer, I., Kikinis, R., Donnino, R., Jolesz, F.A., McCarly, R.W., 1998. Volumetric evaluation of the thalamus in schizophrenic male patients using magnetic resonance imaging. Biol. Psych. 43, 649–659.

Rauch, S.L., Whalen, P.J., Curran, T., Shin, L.M., Coffey, B.J., Savage, C.R., McInerney, S.C., Baer, L., Jenike, M.A., 2001. Probing striatothalamic function in obsessive–compulsive disorder and Tourette syndrome using neuroimaging methods. Adv. Neurol. 85, 207–224.

Reese, T.G., Weisskoff, R.M., Smith, R.N., Rosen, B.R., Dinsmore, R.E., Wedeen, V.J., 1995. Imaging myocardial fiber architecture in vivo with magnetic resonance. Magn. Reson. Med. 34, 786–791.

Rise, M.E., Okada, Y.C., Nicholson, C., 1993. Anisotropic and heterogeneous diffusion in the turtle cerebellum. Implications for volume transmission. J. Neurophys. 70, 2035–2044.

Rubia, K., Russell, T., Bullmore, E.T., Soni, W., Brammer, M.J., Simmons, A., Taylor, E., Andrew, C., Giampietro, V., Sharma, T., 2001. An fMRI study of reduced left prefrontal activation in schizophrenia during normal inhibitory function. Schizophr. Res. 52, 47–55.

Rutherford, M.A., Cowan, F.M., Manzur, A.Y., Dubowitz, L.M. S., Pennock, J.M., Hajnal, J.V., Young, I.R., Bydder, G.M., 1991. MR imaging of anisotropically restricted diffusion in the brain of neonates and infants. J. Comput. Assist. Tomogr. 15, 188–198.

Sakuma, H., Nomura, Y., Takeda, K., Tagami, T., Nakagawa, T., Tamagawa, Y., Ishii, Y., Tsukamoto, T., 1991. Adult and neonatal human brain: diffusional anisotropy and myelination with diffusion-weighted MR imaging. Radiology 180, 229–233.

Samra, K., Riklan, M., Levita, E., Cooper, I.S., 1971. Psychological correlates of anatomically verified thalamic lesions in Parkinsonians. J. Nerv. Ment. Dis. 152, 96–105.

Scannell, J.W., Burns, G.A.P.C., Hilgetag, C.C., O'Neil, M.A., Young, M.P., 1999. The connectional organization of the cortico-thalamic system of the cat. Cereb. Cort. 9, 277–299.

Shimony, J.S., McKinstry, R.C., Akbudak, E., Aronovitz, J.A., Snyder, A.Z., Lori, N.F., Conturo, T.E., 1999. Quantitative diffusion-tensor anisotropy brain MR imaging: normative human data and anatomic analysis. Radiology 212, 770–784.

Smeets, W.J.A.J., de Vos, K., Pool, C.W., Zilles, K., Uylings, H.B.M., 1999. 3-D Cytoarchitectonic parcellation of the human thalamus: correlation with postmortem MRI. Proceedings of the Fifth International Conference on Functional Mapping of the Human Brain 239.

Staal, W.G., Hulshoff, H.E., Schnack, H., van der Schot, A.C., Kahn, R.S., 1998. Partial volume decrease of the thalamus in relatives of patients with schizophrenia. Am. J. Psych. 155, 1784–1786.

Takeda, K., Nomura, Y., Sakuma, H., Tagami, T., Okuda, Y., Nakagawa, T., 1997. MR assessment of normal brain development in neonates and infants: comparative study of T1- and diffusion-weighted images. J. Comput. Assist. Tomogr. 21, 1–7.

Talairach, J., David, M., Tournoux, P., Corredor, H., Kvasina, T. 1957. Atlas d'Anatomie Stéréotaxique. Repérage Radiologique Indirect des Noyaux Gris Centraux, des Régions Mésencéphalo-sous-Optique et Hypothalamique de l'Homme. Masson & Cie, Paris.

Tasker, R.R., Dostrovsky, J.O., Dolan, E.J., 1991. Computerized tomography (CT) is just as accurate as ventriculography for functional stereotactic thalamotomy. Stereotact. Funct. Neurosurg. 57, 157–166.

Tornqvist, A.L., 2001. Neurosurgery for movement disorders. J. Neurosci. Nurs. 33, 79–82.

Van Buren, J.M., Borke, R.C., 1972. Variations and Connections of the Human Thalamus 2. Springer-Verlag, New York.

Virta, A., Barnett, A., Pierpaoli, C., 1999. Visualizing and characterizing white matter fiber structure and architecture in the human pyramidal tract using diffusion tensor MRI. Magn. Reson. Imag. 17, 1121–1133.

Volz, H., Gaser, C., Hager, F., Rzanny, R., Ponisch, J., Mentzel, H., Kaiser, W.A., Sauer, H., 1999. Decreased frontal activation in schizophrenics during stimulation with the continuous performance test—a functional magnetic resonance imaging study. Eur. Psychiatry 14, 17–24.

Vorísek, I., Syková, E., 1997. Evolution of anisotropic diffusion in the developing rat corpus callosum. J. Neurophys. 78, 912–919.

Vuilleumier, P., Chicherio, C., Assal, F., Schwartz, S., Slosman, D., Landis, T., 2001. Functional neuroanatomical correlates of hysterical sensorimotor loss. Brain 124, 1077–1090.

Wiegell, M.R., Larsson, H.B.W., Wedeen, V.J., 1999. Diffusion tensor MRI of the thalamus: differentiation of nuclei by their projections. Proceedings of the International Society for Magnetic Resonance in Medicine 934.

Wiegell, M.R., Larsson, H.B. W., Wedeen, V.J., 2000a. Fiber crossing in human brain depicted with diffusion tensor MR imaging. Radiology 217, 897–903.

Wiegell, M.R., Tuch, D.S., Larsson, H.B.W., Wedeen, V.J., 2000b. Automatic identification of thalamic nuclei from DTI. Proceedings of the Sixth International Conference on Functional Mapping of the Human Brain 6490.

Wimberger, D.M., Roberts, T.P., Barkovich, A.J., Prayer, L.M., Moseley, M.E., Kucharczyk, J., 1995. Identification of "premyelination" by diffusion weighted MRI. J. Comput. Assist. Tomogr. 19, 28–33.

Xuereb, J.H., Perry, R.H., Candy, J.M., Perry, E.K., Marshall, E., Bonham, J.R., 1991. Nerve cell loss in the thalamus in Alzheimer's disease and Parkinson's disease. Brain 114, 1363–1379.